Nuclear Inst. and Methods in Physics Research, A 1000 (2021) 165231

Contents lists available at ScienceDirect

Nuclear Inst. and Methods in Physics Research, A

journal homepage: www.elsevier.com/locate/nima

Scintillation properties and timing performance of state-of-the-art $Gd_3Al_2Ga_3O_{12}$ single crystals

Loris Martinazzoli [a,b,*], Nicolaus Kratochwil [a,c], Stefan Gundacker [a,b,d], Etiennette Auffray [a]

[a] CERN, Esplanade des Particules 1, 1211 Genéve, Switzerland
[b] Universitá degli Studi di Milano-Bicocca, Piazza dell'Ateneo Nuovo, 20126 Milano, Italy
[c] University of Vienna, Universitaetsring 1, 1010 Vienna, Austria
[d] PMI ExMI RWTH Aachen University, Forckenbeckstrasse 55, 52074 Aachen, Germany

ARTICLE INFO

Keywords:
Scintillating crystals
Garnets
Calorimetry
Radiation detection
Neutron detection
Gamma spectroscopy

ABSTRACT

Future colliders will set stringent requirements on the performance of detector materials in terms of timing and radiation hardness. Scintillating garnet crystals proved to satisfy the latter, while the former can be improved through technological developments. In this work, optical and scintillation properties of Cerium-doped $Gd_3Al_2Ga_3O_{12}$ (GAGG:Ce) single crystals were studied upon gamma radiation excitation. Several 2x2x3 mm^3 and 2x2x10 mm^3 samples from various producers were characterized in terms of light output, transmission, scintillation kinetics and coincidence time resolution (CTR). Light output was measured using a ^{137}Cs radioactive source, ranging between 27900 and 49500 photons per MeV. Scintillation emission time profiles were measured with 511 keV gamma excitation, and the fastest samples displayed components below 70 ps rise time and 50 ns decay time. CTR was measured employing silicon photomultipliers (SiPMs) obtaining a best value of 87 ± 2 ps full width at half max[illegible] on past state-of-the-art GAGG.

1. Introduction

Single crystals of Cerium-doped $Gd_3Al_2Ga_3O_{12}$ (GAGG:Ce) showcased scintillation properties of interest for radiation detection [1,2]. Their light yield is higher than BGO's and comparable to NaI's [3], while scintillation decay time is faster than both when co-doped with divalent ions like Mg^{2+} [4,5].

GAGG is a ternary compound of the aluminium garnets, which include notably the binary compounds YAG and LuAG. Gadolinium and Gallium give GAGG a density of approximately 6.6 g/cm^3 and increase the atomic number with respect to YAG:Ce, while keeping the slow scintillation decay time component smaller than that of LuAG:Ce [6]. Moreover, no radioactive background is present in GAGG, which is convenient for X-ray and gamma spectroscopy. Finally, thanks to the large neutron-capture cross section of the Gd isotopes, GAGG can be employed for thermal-neutron detection [7].

Garnet crystals demonstrated excellent radiation hardness to both gamma [8] and hadron radiation [9] – the latter tested up to 1 MGy [10] – and attractive time resolution to minimum-ionizing particles [11], making them valid candidates for detectors at future colliders. Their relative ease of machining and handling, also thanks to the lack of hygroscopicity, combined with their transparency and long attenuation length facilitates employment in high aspect-ratio geometry detectors. One prominent example are fibres in spaghetti calorimeters (SPACAL) [12], which are being considered for the upgrade of the LHCb experiment electromagnetic calorimeter [13].

This work aims to give an overview of the current performance of GAGG crystals from different producers, with a particular focus on fast timing.

First, photoluminescence emission and absorbance spectra are reported. Then, scintillation properties are analysed and discussed. Light output upon gamma excitation was evaluated and energy resolution computed, being two parameters of paramount importance in gamma spectroscopy. The scintillation emission time profile was precisely measured allowing to determine the intrinsic rise and decay times of the crystals. Timing performance of the samples was assessed measuring coincidence time resolution (CTR), i.e. the time resolution achieved measuring the difference in time of arrival of the signals produced by two 511 keV gamma photons emitted in coincidence upon positron annihilation. Recent R&D activities reached values well below 100 ps FWHM [14] and demonstrated that the CTR is closely related to the time resolution achievable in detection of charged particles [15,16]. A concluding discussion of the results and correlations between these quantities will be given, highlighting the role of light output and scintillation kinetics in time resolution.

Given that an electromagnetic shower comprises for a large fraction secondary particles of energy below 1 MeV [17], low-energy gamma

* Corresponding author at: CERN, Esplanade des Particules 1, 1211 Genéve, Switzerland.
E-mail address: loris.martinazzoli@cern.ch (L. Martinazzoli).

https://doi.org/10.1016/j.nima.2021.165231
Received 16 December 2020; Received in revised form 7 March 2021; Accepted 8 March 2021
Available online 13 March 2021
0168-9002/

Table 1
Table of the GAGG crystals characterized in this study, including producers and geometries. The doping is explicitly stated when known.

Name	Producer	Dopants	Geometries
C&A :Ce:Mg	C&A	Ce, Mg	$2 \times 2 \times 3$ mm^3
C&A GFAG	C&A	N/A	$2 \times 2 \times 3$–10 mm^3, $10 \times 10 \times 10$ mm^3
C&A Test 1	C&A	Ce, Mg	$2 \times 2 \times 3$ mm^3
C&A Test 2	C&A	Ce, Mg	$2 \times 2 \times 3$ mm^3
Crytur	Crytur	N/A	$2 \times 2 \times 3$ mm^3
EPIC	Epic-Crystal	N/A	$2 \times 2 \times 3$ mm^3
EPIC fast	Epic-Crystal	N/A	$2 \times 2 \times 3$–10 mm^3
Fomos	Fomos-Materials	Ce, Mg, Ti	$2 \times 2 \times 3$ mm^3
ILM	Institut Lumière Matière	N/A	$2 \times 2 \times 3$–10 mm^3
Siccas :Ce	Siccas	Ce	$2 \times 2 \times 3$ mm^3
Siccas :Ce:Mg	Siccas	Ce, Mg	$2 \times 2 \times 3$ mm^3
Sichuan Tianle	Sichuan Tianle Photonics	N/A	$2 \times 2 \times 3$ mm^3

N/A = Information not available.

sources provide an accessible probe into the properties of the scintillators and their contribution to the performance of high energy physics detectors. Consequently they are, for instance, a valuable input to Monte Carlo simulations.

2. Materials and methods

2.1. Crystal samples

The GAGG crystals characterized in this study are listed in Table 1. Most are products commercially available, and the dopants are stated when known. Gadolinium Fine Aluminium Gallate (GFAG) is a GAGG developed by C&A.

The crystals were grown with Czochralski technique and cut from the ingot to pixels of $2 \times 2 \times 3$ mm^3 and $2 \times 2 \times 10$ mm^3. All of them were mirror-polished except for the C&A samples, which were chemically etched. The latter process was not sufficient for transmission measurements. As an alternative for GFAG, a $10 \times 10 \times 10$ mm^3 mirror-polished cube of the same ingot was used to measure transmission. However, to reduce a possible source of uncertainty for CTR and light output, the polishing of the GFAG samples was improved mechanically at CERN.

2.2. Photoluminescence emission spectrum

Photoluminescence spectra were measured between 470 nm and 870 nm with a Perkin Elmer LS55 Spectrofluorometer. The samples were excited by a 450 nm light beam.

2.3. Transmission and absorbance

A Perkin Elmer Lambda 650 spectrophotometer was employed. A monochromatic light beam was split into two, one used as reference and the other traversing the sample under test. Transmission T is defined as the ratio between the power detected by the instrument measuring this light beam with and without sample.

Absorbance A was computed according to

$$A = -\log_{10} T \tag{1}$$

The minimum transmission detectable by the spectrometer was 0.3%, hence limiting the absorbance at 2.5.

2.4. Light output

The $2 \times 2 \times 3$ mm^3 samples were wrapped in Teflon and coupled with Rhodorsil optical grease (index of refraction n = 1.41) to the photocathode of a Hamamatsu R2059 photomultiplier tube (PMT) placed in a temperature-controlled dark box (20 °C). A ^{137}Cs source was placed 5 cm above the samples. The PMT current signal for each scintillation event was integrated over a gate of 1.5 μs and plotted in a charge histogram normalized to the single photoelectron charge and corrected for the quantum efficiency of the PMT weighted by the photoluminescence spectra (see Section 2.2). Weighted quantum efficiencies ranged from 7.5% to 8%.

2.5. Scintillation kinetics

The set-up for rise and decay time measurements is based on time correlated single photon counting (TCSPC) [18] wherein additionally the energy deposited in both start and stop detector was measured. The test bench is described in detail in [19] and [20]. The start detector consists of a $2 \times 2 \times 5$ mm^3 LSO:Ce crystal co-doped with 0.4% Ca wrapped in Teflon and mounted on a Hamamatsu S13360-3050CS SiPM with Cargille Meltmount optical glue (n = 1.58). The SiPM signal was split, with one branch fed into a NINO ASIC ultrafast discriminator [21] to get the timestamp of the event, and the other used to measure the energy deposition [22] . As stop detector a single photon avalanche diode (SPAD) with 50×50 μm^2 by ID-Quantique (IDQ) ID100-50 was used, selected for its low dark count rate down to 20 Hz. Additionally the crystal under test was placed on a 3×3 mm^2 PM3350 SiPM from Ketek to evaluate the energy deposition for each coincidence. The impulse response function (IRF) of the detection chain was measured exploiting Cherenkov photons produced by photoelectrons in a $2 \times 2 \times 5$ mm^3 PbF_2 crystal painted black on all sides except that facing the IDQ. PbF_2 does not scintillate and it is a good Cherenkov radiator thanks to its high refractive index and wide transparency region. The black paint was used to shield stray light emitted by the Ketek SiPM, and to suppress reflections inside the crystal [23], thus allowing to precisely measure the IRF of the detection chain. The IRF was well-described by a Gaussian with 52 ps standard deviation.

TCSPC systems need a low expectation value λ of the fraction of gamma interactions in the crystal giving rise to a detected signal by the stop detector (the IDQ). In order to assure a correctly measured and not biased scintillation profiles, especially for long decay times, we reduced the solid angle coverage to achieve a $\lambda = 0.01$, measured triggering on the start detector and the Ketek SiPM and recording the IDQ detection rate, sufficiently low to reduce biases to negligible levels [24,25].

The scintillation time profile was mathematically described with a multi-component bi-exponential function:

$$f(t|\theta) = \Theta(t-\theta) \sum_{i=1}^{N} \frac{e^{-(t-\theta)/\tau_{d,i}} - e^{-(t-\theta)/\tau_{r,i}}}{\tau_{d,i} - \tau_{d,r}} \cdot \rho_i \tag{2}$$

where ρ_i is the relative abundance of the ith component, θ the start time of the scintillation process, and $\Theta(t)$ the Heaviside step function. Data were fitted convolving Eq. (2) with the IRF.

The effective decay time $\tau_{d,eff}$ is defined as:

$$\frac{1}{\tau_{d,eff}} \equiv \sum_{i=1}^{N} \frac{\rho_i}{\tau_{d,i}} \tag{3}$$

2.6. Coincidence time resolution

The CTR test bench was based on the NINO ASIC and is described in detail in [22]. A ^{22}Na source was placed between the sample under test and a reference $2 \times 2 \times 3$ mm^3 LYSO:Ce pixel wrapped with several layers of Teflon and coupled to a HPK S13360-3050PE SiPM with Cargille Meltmount optical glue. The tested crystal was wrapped with Teflon and coupled with Rhodorsil optical grease to another HPK

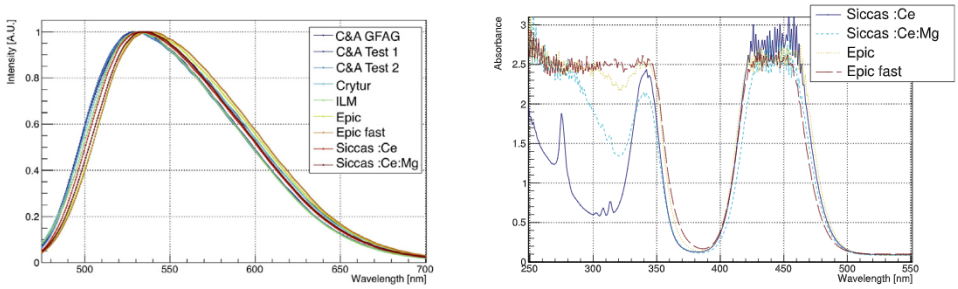

Fig. 1. Left: Photoluminescence emission spectra of all the $2 \times 2 \times 3$ mm^3 samples tested. The spectra span 470 to 700 nm, all peaking in the 520–540 nm range. Right: Absorbance spectra of four typical $2 \times 2 \times 3$ mm^3 samples. They differ mainly below 350 nm: whilst the solely Cerium-doped Siccas shows Gd-related transition peaks, stabilization of Ce^{4+} increases absorption.

Table 2
Light output and energy resolution of the $2 \times 2 \times 3$ mm^3 crystals, upon 661.7 keV excitation with a ^{137}Cs gamma source. The relative uncertainties are ± 3% for the light output and 4% for the energy resolution.

Crystal	Light output [MeV^{-1}]	Resolution (FWHM)
C&A :Ce:Mg	37 280	9.4%
C&A GFAG	32 140	11.3%
C&A Test 1	42 770	7.1%
C&A Test 2	43 100	6.8%
Crytur	29 310	9.9%
EPIC	37 760	11.5%
EPIC fast	30 330	11.5%
Fomos	37 700	11.3%
ILM	27 900	12%
Siccas :Ce	49 500	8.5%
Siccas :Ce:Mg	41 840	6.8%
Sichuan Tianle	38 580	10.8%

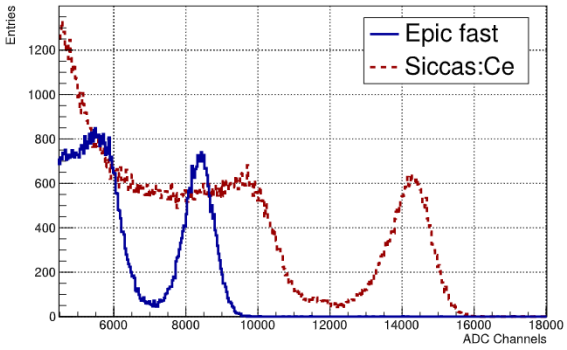

Fig. 2. Light output spectra of the Epic fast and Siccas Cerium-doped sample. The crystal with only Ce-doping shows the highest light output, whilst the stabilization of Ce^{4+} centres speeds up scintillation at the expense of light output.

S13360-3050PE SiPM. Both SiPMs were biased at 60 V, about 8 V overvoltage. As in Section 2.5, the SiPMs' signals were split into two, with one branch fed into the NINO ASIC , whose leading edge delay was the timestamp of the channel, and the other used to measure the energy deposit. Only photopeak events were selected for the measurement. The pulses were digitized with a DRS4 board, 5 GS/s, bandwidth 700 MHz [26]. The histogram of the mutual time delay was produced and fitted with a Gaussian function and its full width at half maximum (FWHM), once corrected for the reference (77 ± 2 ps FWHM), was the contribution of the crystal measured. This, multiplied by $\sqrt{2}$ in the assumption of two identical crystals, is the resulting CTR. For each sample a threshold scan was performed to find the optimal settings.

3. Experimental results

3.1. Optical properties

Photoluminescence spectra are reported in Fig. 1 left. Compatibly with literature values, the spectra span 470 and 700 nm, peaking in the 520–540 nm range. Differences between samples are due to variations in self-absorption and composition, influencing the shape and the peak position of the spectrum, as well as Stokes shift [27].

As mentioned in Section 2, it was not possible to measure transmission of the C&A samples, except for GFAG. All the tested crystals showed a vast transparency region towards the red end of the spectrum starting at approximately 475 nm. Widely known in literature, in the 450–500 nm region emission and absorption overlap producing self-absorption. While being of less importance for $2 \times 2 \times 3$ mm^3 pixels, it is key for high aspect-ratio geometries.

Typical absorbance spectra of the crystals are shown in Fig. 1 right. The two Cerium 4f–5d$_{1,2}$ transition peaks are visible at about 440 and 340 nm. At shorter wavelengths (below ~320 nm) the absorption increases, but differently amongst the samples: the solely Cerium-doped Siccas sample shows a mild slope which steepens for the other samples; because of that, the Gadolinium transition peaks below 320 nm become unresolved. The increased absorption can be attributed to the charge transfer process, clear mark of stable Ce^{4+} ions — achieved for instance through divalent-ions co-doping [4]. The 4f–5d$_2$ peak is not resolved for the samples featuring the strongest absorption (see the Epic fast sample) with the dynamic range of the set-up. The presence of the charge transfer absorption leads to profound differences in scintillation properties discussed in the next sections.

Improving the set-up's dynamic range or employing thinner samples could give further insights into the differences in absorbance between these materials.

3.2. Light output

The measured light outputs ranged from 27 900 ± 1100 up to 49 500 ± 2000 photons/MeV, spanning almost a factor 2. They are reported in Table 2, whilst the energy spectra of two samples are plotted in Fig. 2. Variations are mainly due to differences in composition and quality of the samples. Crystals with stronger charge transfer absorption (see Section 3.1) showed a reduced light output. Additionally, the GFAG's light output was measured before and after the optical polishing process done at CERN, finding no difference within the experimental uncertainty.

Likewise, energy resolution varies amongst the samples. No strong correlation is observed with light output (see for instance the two Siccas). Three main contributions determine the energy resolution, namely photostatistics, inhomogeneity of the sample and non-proportionality of the material [28]. The limit given by photostatistics lies between 5% and 7% for the samples with highest and lowest light output respectively. Lower values can be reached improving the quantum efficiency of the photodetector over the crystals' emission spectra. All

Table 3
Scintillation rise and decay times and relative abundances under 511 keV gamma excitation.

Crystal	τ_r [ps]	τ_{d1} [ns]	R_1 [%]	τ_{d2} [ns]	R_2 [%]	$\tau_{d,eff}$ [ns]
C&A :Ce:Mg	70 ± 15	57 ± 3	61 ± 3	196 ± 15	39 ± 3	79 ± 4
C&A GFAG	63 ± 15	41 ± 3	65 ± 3	172 ± 15	35 ± 3	56 ± 4
C&A Test 1	720 ± 30	81 ± 3	62 ± 3	296 ± 15	38 ± 3	112 ± 4
C&A Test 2	501 ± 30	85 ± 3	62 ± 3	302 ± 15	38 ± 3	117 ± 4
Crytur	73 ± 15	49 ± 3	65 ± 3	207 ± 15	35 ± 3	67 ± 4
EPIC	65 ± 15	64 ± 3	67 ± 3	199 ± 15	33 ± 3	82 ± 4
EPIC fast	60 ± 15	42 ± 3	63 ± 3	139 ± 15	37 ± 3	57 ± 4
Fomos	77 ± 15	60 ± 3	58 ± 3	220 ± 15	42 ± 3	86 ± 4
ILM	78 ± 15	42 ± 3	65 ± 3	145 ± 15	35 ± 3	56 ± 4
Siccas :Ce	1178 ± 50	119 ± 3	72 ± 3	306 ± 15	28 ± 3	144 ± 4
Siccas :Ce:Mg	114 ± 15	72 ± 3	62 ± 3	239 ± 15	38 ± 3	98 ± 4
Sichuan Tianle	148 ± 15	62 ± 3	68 ± 3	128 ± 15	32 ± 3	74 ± 4

Table 4
Table of the CTR measurements performed with the NINO set-up [22]. The samples were measured wrapped in Teflon and coupled with Rhodorsil optical grease to HPK S13360-3050PE. The error of the measurement is ± 3 ps.

Crystal	CTR [ps] $2 \times 2 \times 3$ mm^3
C&A :Ce:Mg	123
C&A GFAG	109
C&A Test 1	184
C&A Test 2	175
Crytur	123
EPIC	128
EPIC fast	109
Fomos	129
ILM	116
Siccas :Ce	250
Siccas :Ce:Mg	146
Sichuan Tianle	120

the measurements yielded values above that, marking the presence of other contributions . Although the samples are small, inhomogeneities in some of them leading to local variations in the light output cannot be excluded. Additionally, surface state effects are mitigated by the Teflon wrapping and grease coupling, but non-uniformities of the wrapping could play a role in deteriorating the resolution. However, more importantly, the non-proportionality in the response is related to the energy resolution [29] and it is influenced by the composition of the crystal: for instance, reducing Gallium to a stoichiometric value of 2.4 improves energy resolution but slows scintillation [30]. Further studies are required to conclude on the matter, however it emerges that the performance of GAGG can be adjusted tuning the composition to best suit the requirements of a given application.

3.3. Scintillation kinetics

Scintillation time profiles were measured selecting only events within the photopeak (511 keV) of the tested crystal. They were adequately described by Eq. (2) with 2 decay times and 1 rise time, and results are reported in Table 3. Fig. 3 shows the scintillation time profile for the C&A's GFAG crystal. C&A's GFAG, Epic's fast, and ILM's crystals were fastest, with a decay component close to 40 ns accounting for about two thirds of the emitted light and a slow decay component well below 200 ns, resulting in an effective decay time of about 55 ns. Rise time was close to 70 ps for these samples.

The scintillation kinetics of garnets can vary at lower excitation energies, in the X-ray range [31]. No appreciable difference was found in these measurements selecting only Compton events down to 200 keV.

3.4. Coincidence Time Resolution (CTR)

CTR varied largely between samples, and values are reported in Table 4. Epic's fast GAGG and C&A's GFAG showed a CTR as low as 109 ± 3 ps, whereas the non-codoped Siccas sample reached 250 ± 3 ps.

4. Discussion

4.1. Light output and scintillation kinetics

In Fig. 4 left, the measured light outputs and effective decay times are plotted over constant-ratio lines drawn for reference. Shifts along one of these can be seen as design choices, wherein balance between light output and decay time is sought without changing – barring variations in rise time – the amount of photons per time interval, i.e. the photon time-density.

The two quantities of that plot are correlated, showing that speeding up scintillation entails a loss in light output. The samples do not lay along constant-ratio lines but move towards higher light output-decay time ratios at smaller decay times, thus improving the photon time-density.

The three samples with fastest kinetics – C&A GFAG, Epic's fast GAGG and ILM's GAGG – share compatible absorption spectra, with high charge transfer absorption below 400 nm and unresolved 4f–5d$_2$ peak (see Figs. 1 right and 4 right). Stabilization of Ce ions in their 4$^+$ state leads to faster scintillation, albeit reducing light output.

Crytur's GAGG, the fourth sample of the bottom left group in Fig. 4 left, features slightly slower scintillation. This could be explained by lower charge transfer, given the less steep slope below 350 nm (Fig. 4 right). Additionally, the 4f–5d$_{1,2}$ Ce peaks are less pronounced, suggesting a lower amount of Cerium.

4.2. CTR and the scintillation parameters

CTR is known to be directly proportional to the square root of the effective decay time $\tau_{d,eff}$ and the rise time τ_r, and inversely proportional to the square root of the number of photons n detected [32]:

$$\mathrm{CTR} \propto \sqrt{\frac{\tau_{d,eff}\,\tau_r}{n}} \tag{4}$$

The number of photons detected n is in fact the light output LO of the crystal multiplied by the photon detection efficiency (PDE) of the photodetector employed $n = \mathrm{LO}\cdot\mathrm{PDE}$. In Fig. 5 the CTR and scintillation parameters are plotted according to Eq. (4), confirming once more the correlation. Error bars are computed by error propagation assuming uncorrelated measurements. The experimental uncertainty on the rise time is a significant contribution to the width of the error bars, and it could be improved reducing the width of the IRF of the set-up.

Efforts are ongoing in the community to obtain an analytical description of the CTR including the photon travel spread (PTS), photodetector single photon time resolution (SPTR), and electronic noise. The PTS is defined as the combined influence of the gamma interaction point fluctuation in the crystal and the time spread of a scintillation photon since its production to the impingement on the photodetector.

A novel analytical model of CTR was recently proposed, leading to the following equation [33]:

$$\begin{aligned}\mathrm{CTR} &\simeq 3.33\sqrt{\frac{\tau_{d,eff}\cdot\left(1.57\cdot\tau_r + 1.13\cdot\sigma_{SPTR*PTS}\right)}{\mathrm{PDE}\cdot\mathrm{LO}}} \\ &= \frac{3.33}{\sqrt{\mathrm{IPTD}}}\end{aligned} \tag{5}$$

where $\sigma_{SPTR*PTS}$ denotes the convolution of the SPTR of the SiPM with the PTS of the crystal, altogether defining the initial photon time-density IPTD. Fig. 6 shows CTR measurements with NINO readout against predictions of Eq. (5), assuming $\sigma_{SPTR*PTS}$ = 62 ps [14] and no electronic contribution. The two agree reasonably well for the fast samples.

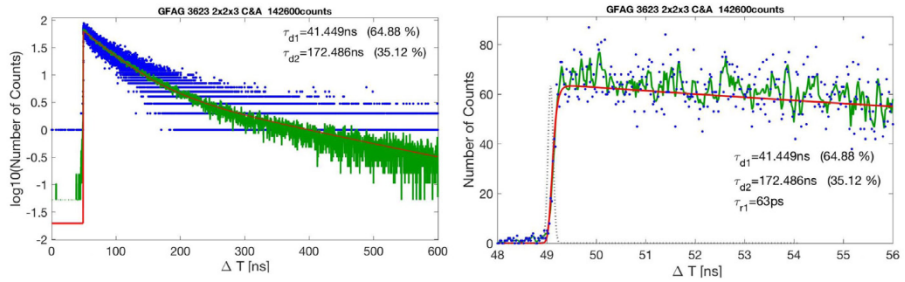

Fig. 3. TCSPC measurement of the GFAG 2 × 2 × 3 mm^3 sample. Blue dots are the measured entries, the red solid line the fitting curve, and the green solid line is a running average of the blue data points as a guide for the eye. The IRF of the system is shown as a black dotted line. Left: log scale plot, highlighting the decay. Right: zoom on the rising edge. (For interpretation of the references to colour in this figure legend, the reader is referred to the web version of this article.)

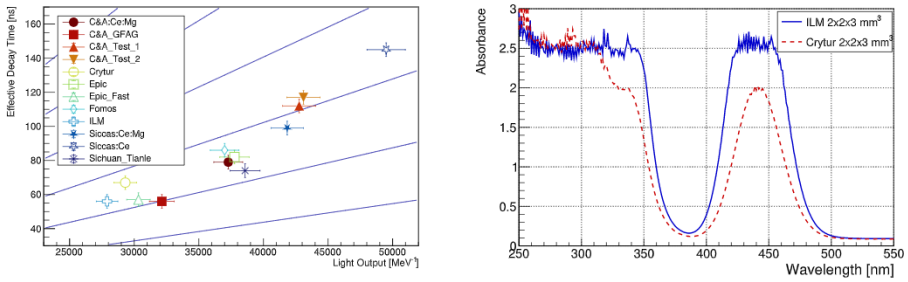

Fig. 4. Left: Effective decay time and light output of the crystals. The blue lines are constant ratios: moving along them grants the same decay time-light output ratio, hence similar timing performance assuming the same rise time. Speeding up scintillation entails a loss of light output, although improving the photon time density. Right: Absorbance spectrum for the ILM and Crytur 2 × 2 × 3 mm^3 crystals. The 4f–5d$_1$ Ce peak (440 nm) is less pronounced for the Crytur's sample and the 4f–5d$_2$ peak (340 nm) resolved, suggesting a lower concentration of Cerium, both in Ce^{3+} and Ce^{4+} state.

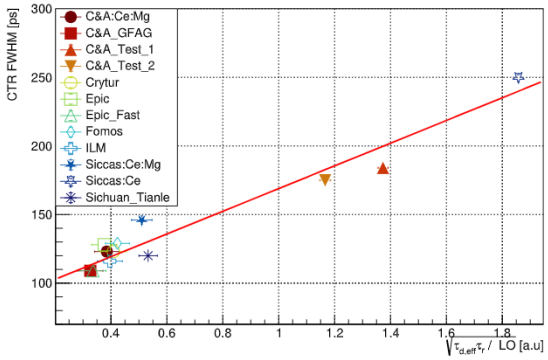

Fig. 5. CTR measured with NINO readout against characteristic rise and decay times and light output as in Eq. (4). The red line is a linear fit to the data (slope 95 ± 2, intercept 80 ± 2), confirming the correlation.

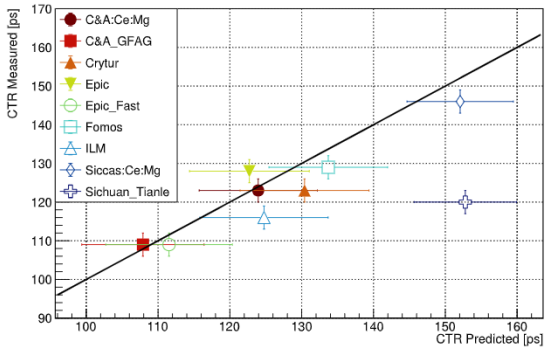

Fig. 6. CTR measured with NINO readout of the fast samples against the theoretical prediction of Eq. (5). The black line is the equivalence between the two axes. The analytic model predicts reasonably well the measurements of the fast samples.

Table 5
Table of the CTR measurements performed with the HF readout [34]. The samples were measured wrapped in Teflon and coupled with Cargille Meltmount optical glue to HPK S13360-3050CS SiPM.

Crystal	CTR (HF) [ps] 2 × 2 × 3 mm^3	CTR (HF) [ps] 2 × 2 × 10 mm^3
C&A :Ce:Mg	99 ± 2	–
C&A GFAG	87 ± 2	124 ± 6
Crytur	101 ± 2	–
EPIC fast	90 ± 2	124 ± 6
ILM	90 ± 2	126 ± 6
Sichuan Tianle	102 ± 3	–
LYSO:Ce [35]	86 ± 2	–

4.3. CTR with high-frequency readout and 10 mm long crystals

In addition to the NINO-based campaign of Section 3.4, the samples showing the best CTR were measured with an experimental high-frequency (HF) bench described in [34]. The goal of this measurements is to assess the gain in performance provided by experimental state-of-the-art readout electronics. In the HF CTR set-up, the NINO chip is replaced by a discrete high-frequency amplifier making the bandwidth of that circuit branch approximately 1.5 GHz. The larger bandwidth allows for better slew rate and higher signal-to-noise ratio, consequently improving timing. The crystals were measured as described in Section 2.6, coupled to HPK S13360-3050CS SiPMs, whose signal was digitized by a 4-channel LeCroy DDA735Zi oscilloscope (3.5 GHz bandwidth, 20 Gs/s sampling rate). The results are shown in Table 5; Epic's fast GAGG, C&A's GFAG, and ILM's GAGG performed similarly within the measurement uncertainty, reaching 90, 87 and 90 ps ± 2 ps. To put these values in context, a CTR of 86 ± 2 ps for LYSO:Ce (The standard material for Time-of-Flight PET) was measured in the same configuration [35].

In view of Eq. (5), a lower electronic noise and $\sigma_{SPTR*PTS}$ could explain the better CTR achieved with the HF and NINO readout.

Additionally, the CTR of three $2 \times 2 \times 10$ mm^3 GAGG pixels was measured. The average CTR degradation observed going from $2 \times 2 \times 3$ mm^3 to $2 \times 2 \times 10$ mm^3 scintillators was 36 ps $\pm$ 3 ps (or 87 ps $\pm$ 4 ps in quadrature), compatible with the results of [36]. This degradation is due to the lower light transfer efficiency, effectively reducing the number of photons detected, and the larger PTS, increasing the time spread of the optical photons.

5. Conclusions

The goal of this work was to explore and understand the current scintillation performance of cerium-doped GAGG single crystals as radiation detectors, testing several samples from various producers.

Light output between 27 900 and 49 500 photons/MeV was measured upon 661.7 keV ^{137}Cs gamma excitation. The scintillation time profiles could be parameterized with a bi-exponential function featuring a single characteristic rise time and two decay times, a fast and a slow one as low as 42 ns and 139 ns. The effective decay time of the samples ranged from 56 ns to 144 ns. The best CTR achieved was 87 $\pm$ 2 ps.

Large variations between samples were observed. Light output and effective decay time spanned almost a factor 2 and 3, respectively. Such differences are down to two reasons: growth conditions and design choices. On the one hand, importance of growth conditions is visible in the two C&A test samples: although both Mg-codoped, they present a slow pulse with an effective decay time closer to a non-codoped one. On the other hand, crystal engineering of GAGG offers a handle to finely tune the scintillation properties according to the applications' requirements. For instance, while gamma ray spectroscopy and neutron detection can profit from high light output and good energy resolution, fast scintillation is instrumental to mitigate pile-up in a high-rate environment, e.g. at future colliders.

Although not as fast and with a high stopping power as L(Y)SO, radiation hardness proven up to 1 MGy with protons and large light output make this material outstanding. GAGG emerges as a mature technology and a promising candidate for high-radiation environments, neutron detection, gamma ray spectroscopy, and scintillation-based particle detectors at future high-luminosity colliders.

CRediT authorship contribution statement

Loris Martinazzoli: Formal analysis, Investigation, Methodology, Software, Validation, Writing - original draft, Conceptualization, Writing - review & editing. **Nicolaus Kratochwil:** Investigation, Validation, Conceptualization, Writing - review & editing. **Stefan Gundacker:** Methodology, Software, Conceptualization, Writing - review & editing. **Etiennette Auffray:** Resources, Supervision, Conceptualization, Writing - review & editing.

Declaration of competing interest

The authors declare that they have no known competing financial interests or personal relationships that could have appeared to influence the work reported in this paper.

Acknowledgements

This work was performed in the framework of the Crystal Clear collaboration. The authors would like to thank Dr. K. Lebbou from ILM, and the producers C&A, Crytur, Fomos-Materials, Siccas, and Sichuan Tianle Photonics for kindly providing their samples, as well as Dominique Deyrail for polishing the C&A GFAG crystal.

References

[1] K. Kamada, et al., Composition engineering in Cerium-doped (Lu, Gd)$_3$(Ga, Al)$_5$O$_{12}$ single-crystal scintillators, Cryst. Growth Des. 11 (2011) 4484–4490.
[2] K. Kamada, et al., 2-inch size single crystal growth and scintillation properties of new scintillator; Ce:Gd$_3$Al$_2$Ga$_3$O$_{12}$, IEEE Nucl. Sci. Symp. Conf. Rec. (2011).
[3] C. van Eijk, Inorganic scintillators in medical imaging, Phys. Med. Biol. 47 (2002) R85–R106.
[4] K. Kamada, et al., Alkali earth co-doping effects on luminescence and scintillation properties of Ce doped Gd$_3$Al$_2$Ga$_3$O$_{12}$ scintillator, Opt. Mater. 41 (2015) 63–66.
[5] M.T. Lucchini, et al., Effect of Mg^{2+} ions co-doping on timing performance and radiation tolerance of cerium doped Gd$_3$Al$_2$Ga$_3$O$_{12}$ crystals, NIM A 816 (2016) 176–183.
[6] M. Nikl, et al., Development of LuAG-based scintillator crystals - A review, Prog. Cryst. Growth Charact. Mater. 59 (2) (2013) 47–72.
[7] M.P. Taggart, M. Nakhostin, P.J. Sellin, Investigation into the potential of GAGG:Ce as a neutron detector, NIM A 931 (2019) 121–126.
[8] M.T. Lucchini, et al., Et al radiation tolerance of LuAG:Ce and YAG:Ce crystals under high levels of gamma- and proton-irradiation, IEEE Trans. Nucl. Sci. 63 (2016) 2.
[9] E. Auffray, et al., Irradiation effects on Gd$_3$Al$_2$Ga$_3$O$_{12}$ scintillators prospective for application in harsh irradiation environments, Rad. Phys. Chem. 164 (2019) 108365.
[10] V. Alenkov, et al., Irradiation studies of a multi-doped Gd$_3$Al$_2$Ga$_3$O$_{12}$ scintillator, NIM A 916 (2019) 226–229.
[11] M.T. Lucchini, et al., Timing capabilities of garnet crystals for detection of high energy charged particles, NIM A 852 (2017) 1–9.
[12] K. Pauwels, et al., Single crystalline LuAG fibers for homogeneous dual-readout calorimeters, JINST 8 (2013) P09019.
[13] L. Martinazzoli, Crystal fibers for the LHCb calorimeter upgrade, IEEE Trans. Nucl. Sci. 67 (6) (2020) 1003–1008, http://dx.doi.org/10.1109/TNS.2020.2975570.
[14] S. Gundacker, et al., Experimental time resolution limits of modern SiPMs and TOF-PET detectors exploring different scintillators and cherenkov emission, Phys. Med. Biol. 65 (2020) 025001.
[15] A. Benaglia, et al., Detection of high energy muons with sub-20 ps timing resolution using L(Y)SO crystals and SiPM readout, NIM A 830 (2016) 30–35.
[16] CMS Collaboration, A MIP timing detector for the CMS phase-2 upgrade, 2019.
[17] R. Wigmans, Calorimetry – Energy Measurement in Particle Physics, second ed., in: International Series of Monographs on Physics, vol. 168, Oxford University Press, 2017.
[18] L. Bollinger, G. Thomas, Measurement of the time dependence of scintillation intensity by a delayed-coincidence method, Rev. Sci. Instrum. 32 (1961) 1044–1050.
[19] S. Gundacker, et al., Measurement of intrinsic rise times for various L(Y)SO and LuAG scintillators with a general study of prompt photons to achieve 10 ps in TOF-PET, Phys. Med. Biol. 61 (2016) 2802–2837, http://dx.doi.org/10.1088/0031-9155/61/7/2802.
[20] S. Gundacker, et al., Precise rise and decay time measurements of inorganic scintillators by means of X-ray and 511 keV excitation, NIM A 891 (2018) 42–52.
[21] F. Anghinolfi, et al., NINO: An ultrafast low-power front-end amplifier discriminator for the time-of-flight detector in the ALICE experiment, IEEE Trans. Nucl. Sci. 51 (2004) 1974.
[22] S. Gundacker, et al., Time of flight positron emission tomography towards 100 ps resolution with L(Y)SO: an experimental and theoretical analysis, JINST 8 (2013) P07014.
[23] N. Kratochwil, et al., On the experimental time resolution limits of sole Cherenkov radiators with SiPMs in TOF-PET, Phys. Med. Biol. (2021) submitted for publication.
[24] S. Seifert, et al., Accurate measurement of the rise and deca ytimes of fast scintillators with solid state photon counters, JINST 7 (2012) P09004.
[25] S.E. Derenzo, et al., Measurements of the intrinsic rise times of common inorganic scintillators, IEEE Trans. Nucl. Sci. 47 (2000) 3.
[26] S. Ritt, Design and performance of the 6 GHz waveform digitizing chip DRS4, IEEE Nucl. Sci. Conf. Rec. (2008) 1512–1515.
[27] K. Kamada, et al., Scintillator-oriented combinatorial search in Ce-doped (Y, Gd)$_3$(Ga, Al)$_5$O$_{12}$ multicomponent garnet compounds, J. Phys. D: Appl. Phys. 44 (2011) 505104.
[28] P. Dorenbos, Fundamental limitations in the performance of Ce^{3+}-Pr^{3+}-, and Eu^{2+}-activated scintillators, IEEE Trans. Nucl. Sci. 57 (2010) 3.
[29] I.V. Khodyuk, et al., Nonproportional response between 0.1–100 kev energy by means of highly monochromatic synchrotron X-rays, IEEE Trans. Nucl. Sci. 57 (2010) 3.
[30] K. Kamada, et al., Cz grown 2-in. size Ce:Gd$_3$(Al, Ga)$_5$O$_{12}$ single crystal; relationship between Al, Ga site occupancy and scintillation properties, Opt. Mater. 36 (2014) 1942–1945.
[31] A. Belsky, et al., Mechanisms of luminescence decay in YAG-Ce, Opt. Mater. 92 (2019) 341–346.
[32] S. Gundacker, Time Resolution in Scintillator Based Detectors for Positron Emission Tomography Ph.D. thesis, Vienna University of Technology, 2014.

[33] S. Vinogradov, Approximations of coincidence time resolution models of scintillator detectors with leading edge discrimination, NIM A 912 (2018) 149–153.
[34] S. Gundacker, et al., High-frequency SiPM readout advances measured coincidence time resolution limits in TOF-PET, Phys. Med. Biol. 64 (2019) 055012.
[35] Stefan Gundacker, Arjan Heering, The silicon photomultiplier: fundamentals and applications of a modern solid-state photon detector, Phys. Med. Biol. 65 (2020) 17TR01.
[36] S. Gundacker, et al., Time resolution deterioration with increasing crystal length in a TOF-PET system, NIM A 92–100 (2014) 737.